PAPER

Electronic and thermal properties of non-stoichiometric and doped cobaltum antimonide

Materials Research Express

RECEIVED
9 January 2018

REVISED
5 February 2018

ACCEPTED FOR PUBLICATION
15 February 2018

PUBLISHED
28 February 2018

PAPER

Electronic and thermal properties of non-stoichiometric and doped cobaltum antimonide

Diego Velasco-Soto[1], **Eduardo Menéndez-Proupin**[1], **Rebeca Realyvazquez-Guevara**[2] and **José Andrés Matutes-Aquino**[2]

[1] GMM, Departamento de Física, Facultad de Ciencias, Universidad de Chile, Las Palmeras 3425, 780-0003 Ñuñoa, Santiago, Chile
[2] Centro de Investigación en Materiales Avanzados, Miguel de Cervantes 120, 31136 Chihuahua, Mexico

E-mail: diego.velasco@cimav.edu.mx, eariel99@gmail.com, paula.realyvazquez@cimav.edu.mx and jose.matutes@cimav.edu.mx

Keywords: semiconductors, thermoelectric materials, thermal properties, electric properties, modeling

Supplementary material for this article is available online

Abstract

The electronic, vibrational and thermal properties of stoichiometric and non-stoichiometric cobalt antimonide $CoSb_x$ ($x = 2.81, 2.875$, and 3) are investigated by means of first principle calculations and thermal measurements. The molar heat capacity, electrical conductivity, and the electronic thermal conductivity are increased by the effect of Sb vacancies. Doping with Te and Ge also increases the electrical and thermal conductivity, suggesting that it can be used to enhance cobaltum antimonide as a thermoelectric material.

1. Introduction

In recent times, with the growing demand for energy, special attention has been paid to different technologies related to energy production and saving. In this respect, research in thermoelectric materials is relevant. The thermoelectric materials allow the conversion of heat into electrical energy and vice versa. In the first case, the mechanism for the conversion of heat to energy is explained by the Seebeck effect, and the efficiency of a thermoelectric material is characterized by the figure of merit [1–4].

Thermoelectric materials are good electrical conductors, bad thermal conductors and have a high Seebeck coefficient. Good thermoelectric materials have $ZT \sim 1$ [5–7].

A thermoelectric material that has attracted great interest in the literature is doped cobaltum antimonide, $CoSb_3$. $CoSb_3$ belongs to the family of compounds known as skutterudites, which have the formula TX_3 (T = Co, Rh, Ir and X = P, As, Sb). $CoSb_3$ has a cubic lattice, with the symmetry group 204 ($Im\bar{3}$) and a lattice parameter of 9.1823 Å [8]. The cell consists of 32 atoms and this corresponds to eight formula units. The crystallographic unit cell consists of eight connected octahedra, one for each corner of the cell. In the center of the cells, voids of considerable size are formed, which are known in the literature as 'cages' [9]. The use of $CoSb_3$ as a thermoelectric is due to its high Seebeck coefficient and its high electrical conductivity. However, it has the disadvantage of having a high thermal conductivity. Kurmaev *et al* compared the thermoelectric properties of several skutterudites, in which $CoSb_3$ presented good performance in these same ones [10].

The figure of merit of $CoSb_3$ may be increased by reducing its rather high thermal conductivity. Some ways in which thermal conductivity could be reduced have been explored in the literature [11–14]. One proposal is to include impurity atoms in the sample, i. e. doping with filler atoms (atoms inside the cages). Another way to reduce thermal conductivity is nanostructuring the sample. The reduction of thermal conductivity in this case is due to both the interaction of phonons with the lattice and the presence of quantum size effects [15].

In this work, we study from first principles, the thermal and electrical properties of $CoSb_3$ and related compounds. In particular, were studied the properties of $CoSb_{2.875}$ (obtained by introducing a vacancy in the crystallographic cell, i. e., removing one of the 24 Sb atoms) and the compounds $CoTe_{0.125}Sb_{2.875}$ and $CoGe_{0.125}Sb_{2.875}$ (obtained by substituting one Sb atom in the cell for one of Te and Ge respectively). This paper is structured as follows. Section 2 includes the technical details and is divided in two subsections. The first one

contains details about the *ab initio* calculations and the second one about obtaining the experimental data. Section 3 presents and discusses the results obtained. This is also divided in two subsections. The first subsection deals with the results of electronic structure, especially the band structure and electronic density of states. The second subsection describes the results related to lattice dynamics. In section 4, we present our conclusions.

2. Technical details

2.1. Computational details

The calculations were performed using the density-functional theory (DFT) using the Quantum ESPRESSO software package [16].

The equilibrium lattice parameter was calculated for $CoSb_3$ by determining the energy as a function of the volume of the cell and adjusting the data obtained by means of the Birch-Murnaghan state equation.

$$E(V) = E_0 + \frac{9V_0B_0}{16}\left\{\left[\left(\frac{V_0}{V}\right)^{2/3} - 1\right]^3 B_0' + \left[\left(\frac{V_0}{V}\right)^{2/3} - 1\right]^2\left[6 - 4\left(\frac{V_0}{V}\right)^{2/3}\right]\right\} \quad (1)$$

where E indicates the total energy and V the volume. E_0 indicates the minimum energy and V_0 the volume corresponding to that energy, B_0 is the bulk modulus and B_0' indicates the derivative of the bulk modulus with respect to the pressure.

The band structure and the density of states were determined for $CoSb_3$, $CoSb_{2.875}$, $CoTe_{0.125}Sb_{2.875}$ and $CoGe_{0.125}Sb_{2.875}$. The exchange-correlation funcional of Perdew, Burke and Ernzerhoff (PBE) [17] was used in all the calculations. The electron-core interaction is accounted for by means of norm conserving (Sb) and ultrasoft (Co, Te, Ge) pseudopotentials. The Sb pseudoptential has been taken form the GHHT library [18, 19] available at the Quantum ESPRESSO web site. The Co, Te and Ge ultrasoft pseudpotentials are taken from the SSSP library [20–22]. A convergence study was carried out to determine the parameters to be used in the calculations. Based on this study, a kinetic energy cutoff of 55 Ry was used for the expansion of the wave functions and a 440 Ry cutoff was used for the charge density. The band structure was calculated on the path Γ(0, 0, 0)-X(0.5, −0.5, 0)-M(0.5, 0, 0)-Γ(0, 0, 0)-R(0.5, −0.5, 0.5) in the first Brillouin zone. The density of states (DOS) was computed for the relaxed cell. The structure relaxations were done using a grid of **k**-points ($4 \times 4 \times 4$), followed by DOS calculations using a denser grid of **k**-points ($10 \times 10 \times 10$ k-points). Later, based on the calculation of the electronic structure in a mesh of $10 \times 10 \times 10$ **k**-points, the temperature-dependent electrical conductivity, thermal conductivity and electronic heat capacity, were determined using the Boltzmann's kinetic equation theory, as implemented in the BoltzTrap software package [23].

The phonon calculations were carried out for $CoSb_3$ and $CoSb_{2.875}$ using density functional perturbation theory (DFPT), as implemented in the PHONON code of Quantum ESPRESSO [24]. Before the calculations of the lattice dynamics, the convergence of the dielectric constant and frequencies of several modes was studied. From these studies, the parameters to be used in the calculations were determined (55 Ry for the energy cutoff for the expansion of the wave functions and 440 Ry for the charge densities). A $3 \times 3 \times 3$ **k**-point grid was utilized for the electronic structure calculations. For the lattice dynamics, a $3 \times 3 \times 3$ **q**-point grid was used in the DFPT calculations. The results calculated on this mesh of **q**-points were interpolated to a finer mesh of q-points ($60 \times 60 \times 60$ **q**-points) to obtain the phonon DOS and the heat capacity curves as a function of temperature. The phonon dispersion curve was calculated along the path Γ(0, 0, 0)-M(0.5, −0.5, 0)-X(0.5, 0, 0)-Γ(0, 0, 0)-R(0.5, −0.5, 0.5)-X(0, 0, 0.5).

2.2. Experimental details

Polycrystalline skutterudite ($CoSb_3$) was prepared using a sequence of processes including arc-melting, melt spinning, grounding, cold pressing and annealing. To avoid oxidation, each individual process was carried out under protective Ar atmosphere. Co pieces with a purity of 99.5% (Alfa Aesar) and Sb shoot with a purity of 99.9999% (Alfa Aesar) were used as raw materials. Sb has a low vapor pressure, thus volatilization of Sb during the fabrication of $CoSb_3$ was compensated by adding 10 wt% excess of stoichiometric amount of Sb. As a first step, an arc melting furnace was used to obtain an ingot. Afterwards, the button was re-melted under vacuum in an induction furnace. To obtain the ribbons, the melt was ejected onto the copper wheel of a melt-spinning system, rotating with a tangential velocity of 30 m s^{-1}. The resulting products were a mix of finely divided ribbon flakes and wider ribbon sections. The ribbons were grounded using an agate mortar and the resulting powder was loaded into a die cavity of 8 mm $\times$ 8 mm. Then, the powder was cold pressed under a uniaxial pressure of 5 MPa during 1.5 min. Finally, the resulting green body was annealed at 650 °C during 2 h. The heating and cooling rates were of 10 °C min^{-1}.

The composition was determined by averaging the chemical composition obtained by Energy-Dispersive x-ray (EDX) microanalysis attached to the SEM (JEOL-JSM 5800) and by normalizing the resulting chemical

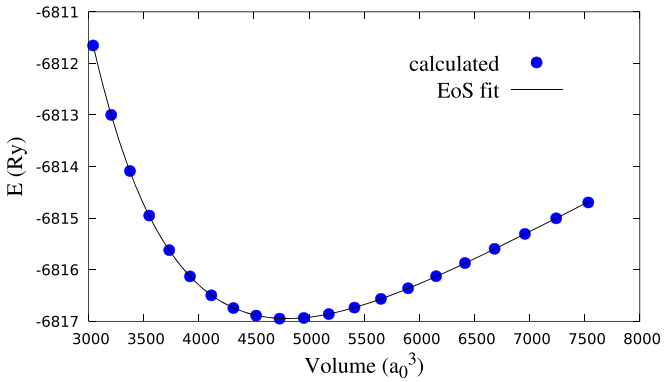

Figure 1. Energy versus volume plot for $CoSb_3$.

Table 1. Data obtained from the adjustment using the Birch-Murnaghan equation of state. The adjustment standard errors are indicated.

Parameter	Value
V_0	4800 ± 2 bohr^3
B_0	101.2 ± 0.1 GPa
B_0'	4.73 ± 0.01

formula to a cobalt atom, which is the element less likely to be lost during the fabrication process. The composition of the sample, as determined by this procedure, was $CoSb_{2.81}$.

The low-temperature specific heat was measured from 5 to 50 K in a PPMS Heat Capacity Option (Quantum Design). This system measures the heat capacity of a sample at constant pressure. To this a fixed amount of heat is applied, the temperature change is observed during a period of time (heating) and subsequently the cooling during a period of time of the same duration. The procedure applied to the sample by means of this same system is as follows. [25] The sample was fixed to the platform by a small amount of Apriezon N grease in order to ensure good thermal contact between the sample and the puck. The specific heat contributions of the puck and of the layer of grease were measured in an addendum run prior the sample measurement and subtracted from the data to obtain the specific heat of the sample. More information about the sample to which the measurements of specific heat were made and more characterizations of the same are detailed in [26].

3. Results and discussion

3.1. Electronic properties

In the following, we present a study of the effect on the electronic structure and properties of the presence of vacancies and substitutional atoms of Ge and Te at the sites of Sb. The electronic properties of skutterudites and the influence of different doping atoms on his properties have been reported in numerous studies. [4–6, 27–33].

The dependence of the total energy as a function of the volume of the cell for $CoSb_3$ is shown in figure 1. This figure shows both the data obtained from the simulations and the adjustment of the data to the Birch-Murnaghan equation. The values of the parameters obtained, as given in equation (1), are shown in table 1, with their statistical uncertainties.

The value of the lattice parameter, predicted by the model, is $a = 8.927$ Å. Different values of the experimental lattice parameter have been cited in the literature. For example Christensen *et al* [8] determined a value of $a = 9.1823$ Å, whereas Arushanov *et al* obtained a value of $a = 9.036$ Å [34]. The discrepancy is 2.8% with respect to the first mentioned value and 1.2% with respect to the second. The result is also consistent with another one cited in the literature and obtained by *ab initio* method [3], for which a value of $a = 8.9234$ Å was obtained. The value of the bulk modulus was also compared with other published results, as shown in table 2.

Table 3 compares our gap value obtained for $CoSb_3$ with other values, obtained in both experimental and *ab initio* studies. There is a considerable dispersion in the results obtained, which is of the order of the DFT accuracy. Defects in the samples also influence the indeterminacy of the values obtained in the experiments.

Table 2. Comparison of the value of the bulk modulus obtained in this study with others reported in the literature.

Value (GPa)	Reference	Method
101.18	This work	DFT/GGA
97.65	[3]	DFT/GGA
93.6	[35]	Experimental
81 ± 1	[36]	Experimental
93.2	[37]	Experimental
85	[38]	DFT/GGA
81.09	[27]	DFT/GGA

Table 3. Comparison of the value of the energy gap for $CoSb_3$ obtained in this study with others reported in the literature.

Value (eV)	Reference	Method
0.124	This work	DFT/GGA
0.05	[39]	DFT/LDA
0.55	[40]	Experimental
0.22	[41]	DFT/LSDA
0.03	[42]	Experimental
0.05	[43]	Experimental
0.14	[10]	DFT/LDA
0.226	[3]	DFT/GGA
0.036	[27]	DFT/GGA
0.118	[38]	DFT/GGA

Figure 2 shows the electronic DOS of $CoSb_3$, $CoSb_{2.875}$, $CoTe_{0.125}Sb_{2.875}$ and $CoGe_{0.125}Sb_{2.875}$. For the last two compositions, the DOS projected at Te and Ge sites (PDOS) are also shown. The straight lines indicate the Fermi level. The compounds in question show a variety of behaviors with respect to their electrical properties. For $CoSb_3$ a very small gap of 0.124 eV is observed, with the Fermi level in the middle of the same, which implies a narrow gap semiconductor behavior. In the non-stoichiometric compound $CoSb_{2.875}$, the bottom of the conduction band gets occupied and the compound becomes a conductor. Moreover, the former valence-conduction gap of the stoichiometric compound closes and cannot be appreciated in the DOS. Figure S1 is available online at stacks.iop.org/MRX/5/025908/mmedia (see Supplemental material) shows the band diagram of both $CoSb_3$ and $CoSb_{2.875}$. It can be appreciated that the well-defined valence and conduction band edges of $CoSb_3$ at the Γ point become considerably modified due to the cobalt vacancies. For the doped composition $CoTe_{0.125}Sb_{2.875}$, the extra electrons provided by Te cause that the Fermi level is just above the conduction band bottom (the compound has electrons as current carriers). Finally, for the composition $CoGe_{0.125}Sb_{2.875}$, the Fermi level is below the valence band maximum, indicating that the current carriers are holes. Figures S1(c) and (d) show the band diagrams of $CoTe_{0.125}Sb_{2.875}$ and $CoGe_{0.125}Sb_{2.875}$, respectively. In these cases the structure of the band edges of $CoSb_3$ is conserved. Our resuls for $CoTe_{0.125}Sb_{2.875}$ are consistent with those of Zhu *et al* [29].

The values of the electrical conductivity, the thermal conductivity and the heat capacity as a function of the temperature (figure 3) were determined in a temperature range of up to 300 K, using the Boltztrap package [23]. For the thermal conductivity and the heat capacity, the calculation includes only the electronic contribution of these magnitudes. The contribution of phonons to the heat capacity will be considered later. In these graphs it is observed that the parent compound has the lowest values of electrical conductivity and electronic thermal conductivity, as expected for an insulator with band gap larger than $k_B T$. The parent compound has the Fermi level within the gap and a very small fraction of the electrons can reach the conduction band to behave as charge and thermal energy carriers. However, for the composition including vacancies ($CoSb_{2.875}$), it is observed that these induce a considerable increase in electrical conductivity. Samples manufactured for experimental studies generally have defects (including vacancies), such as the experimental sample whose measurements are published in this study. This implies that the actual samples exhibit a behavior closer to that of the $CoSb_{2.875}$ composition than to the parent compound, and therefore is expected to exhibit higher thermal conductivity and better efficiency in their thermoelectric properties.

The thermal conductivity, as already mentioned, only includes the contribution of the electrons and not that of the phonons. The thermal conductivity is lower in $CoSb_3$ than in the rest of the compounds. Because

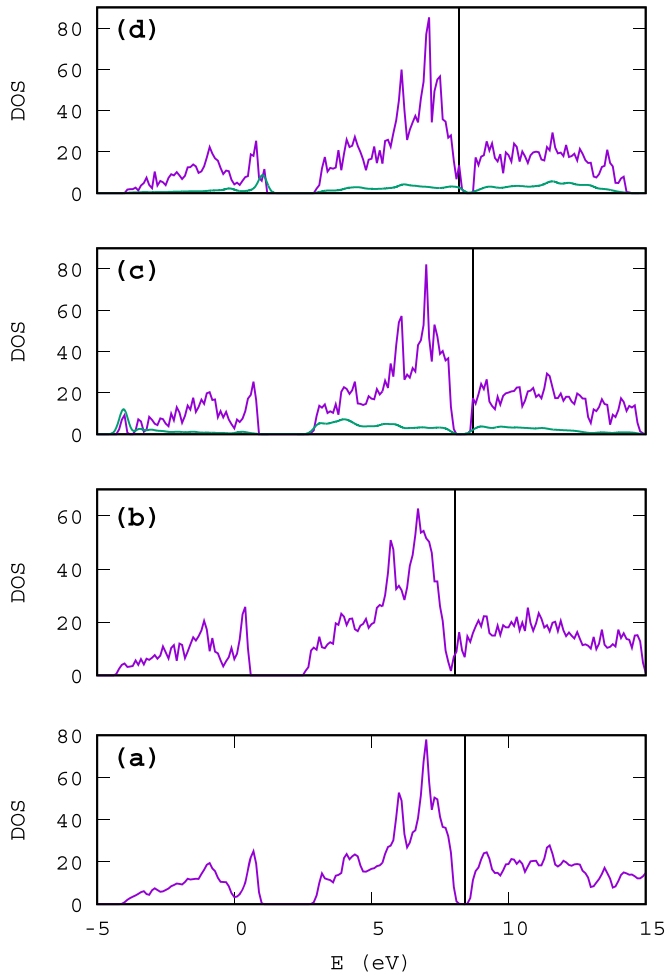

Figure 2. Electronic density of states (DOS) for (a) $CoSb_3$, (b) $CoSb_{2.875}$, (c) $CoTe_{0.125}Sb_{2.875}$ and (d) $CoGe_{0.125}Sb_{2.875}$. The green lines indicate the projected DOS of Te and Ge respectively. The value of the projected DOS was multiplied by a factor of 7.

figure 3(b) includes the contribution of electrons only, this does not contradict what was stated in the introduction that the presence of defects decreases the thermal conductivity.

3.2. Phonon calculations

Figure 4 shows the phonon dispersion curves and the state density for the $CoSb_3$ and $CoSb_{2.875}$ compositions. In both compositions it is observed that the frequencies are clearly separated into two groups. For the $CoSb_3$ there is a gap that spans approximately from 192 to 241 cm^{-1}. For the $CoSb_{2.875}$ there is no gap. *Ab initio* calculations of the skutterudite lattice dynamics have been published in the literature, for example in Feldman *et al* [44, 45], Ghosez and Veithen [46], Lu *et al* [2], Wee *et al* [28] and Volja *et al* [47] Several of the compositions that have been studied in the literature present the behavior reported here, the frequencies in the phonon dispersion curves separated into two groups. However, the effect of introducing vacancies in the $CoSb_3$ on the lattice dynamics has not been studied before. Our results show that the Sb vacancies in $CoSb_{2.875}$ has the effect of closing the gap between these two groups. Our calculation displays some imaginary frequencies near the Γ point, but it has has a negligible effect on the DOS and the thermal properties. The imaginary frequencies just reveal the limitations of modeling a system with disordered vacancies using periodic boundary conditions.

The heat capacity of $CoSb_{2.875}$ was determined as a function of temperature, in a range up to 50 K. Figure 5 includes the contribution to the heat capacity due to the lattice vibrations (phonons) and the contribution due to the electrons for $CoSb_{2.875}$. The curve of the electron contribution is the same as that of figure 3. The electronic contribution to heat capacity in the $CoSb_3$ composition is negligible.

The comparison of the experimental data with our calculation is presented in figure 6. From the calculations it is seen that the vacancies increase the molar heat capacity. This increment is mainly due to the rearrangment of the phonon frequencies, and to a lesser extent, to the electronic contribution only present in $CoSb_{2.875}$. As the vacancy concentration in the computational model is smaller than the experimental value, the heat capacity of $CoSb_{2.875}$ could be expected to be between that for $CoSb_{2.81}$ (experimental) and for stoichiometric $CoSb_3$

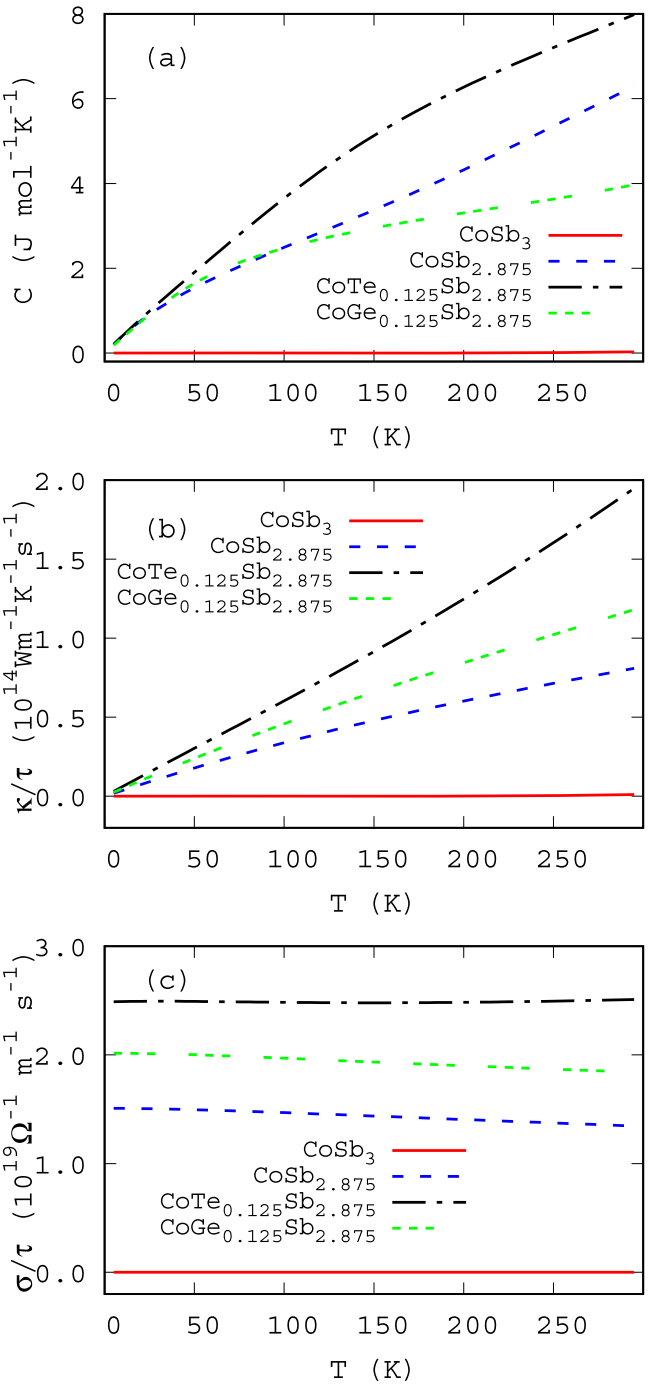

Figure 3. (a) Heat capacity versus temperature for the compositions $CoSb_3$, $CoSb_{2.875}$, $CoTe_{0.125}Sb_{2.875}$ and $CoGe_{0.125}Sb_{2.875}$, (b) electronic thermal conductivity versus temperature, and (c) electric conductivity versus temperature.

(theory). The discrepancy between the experimental curve and the calculated curve could be explained by the fact that in the experimental data C_P (specific heat at constant pressure) was measured, while C_V (specific heat at constant volume) was calculated by Quantum ESPRESSO. The relation between these magnitudes is given by

$$C_P - C_V = VT\frac{\alpha^2}{\beta_T} \tag{2}$$

where α is the volumetric thermal expansion coefficient and β_T is the isothermal compressibility. The difference $C_P - C_V$ tends to zero a with the temperature, not only due to the factor T, but also because α tends to zero at zero temperature [48]. Considering $\alpha \sim 10^{-6}\ K^{-1}$ and approximating $1/\beta_T$ by the isentropic bulk moduls, we get $C_P - C_V \sim 10^{-4}$ J mol^{-1} K, not explaining the difference between the experimental and the calculated values. Therefore, the discrepancy could be explained by the errors inherent to the calculations, or maybe the heat capacity does not depend monotonically with the vacancy concentration. The very small or negligible

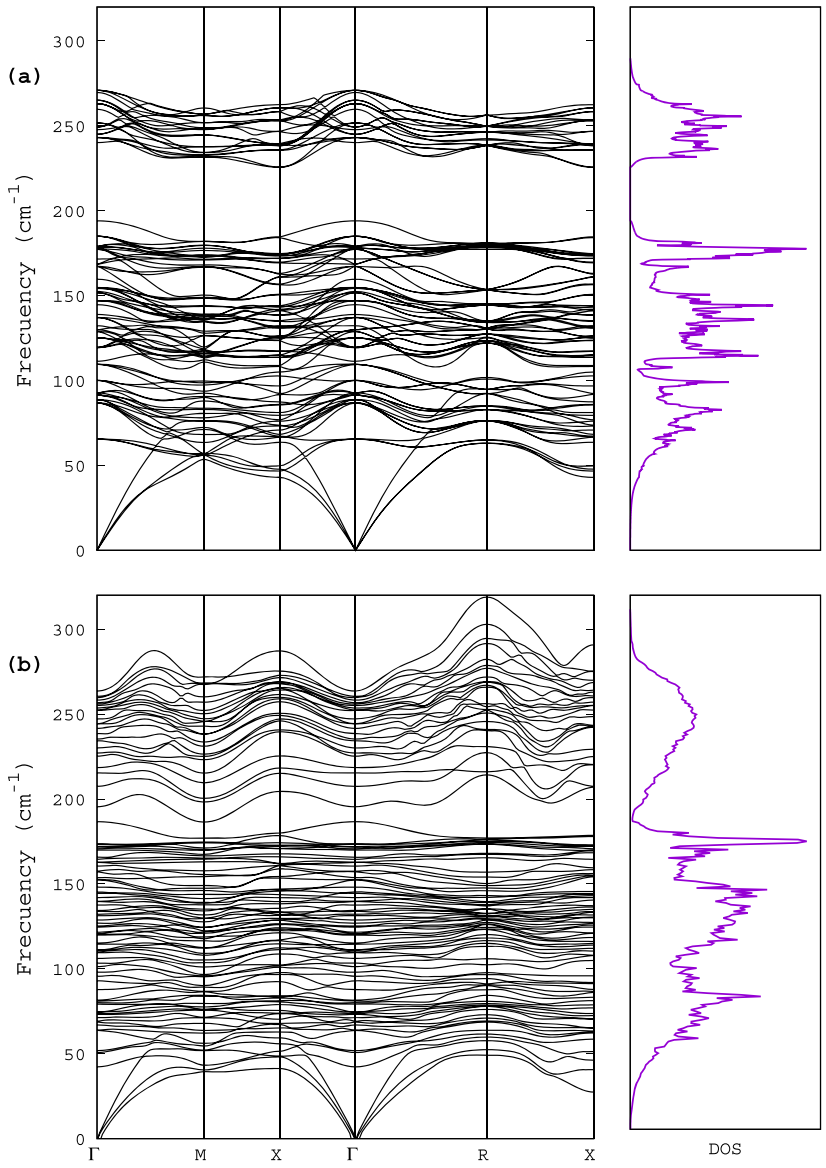

Figure 4. Phonon dispersion curves for (a) $CoSb_3$, y (b) $CoSb_{2.875}$.

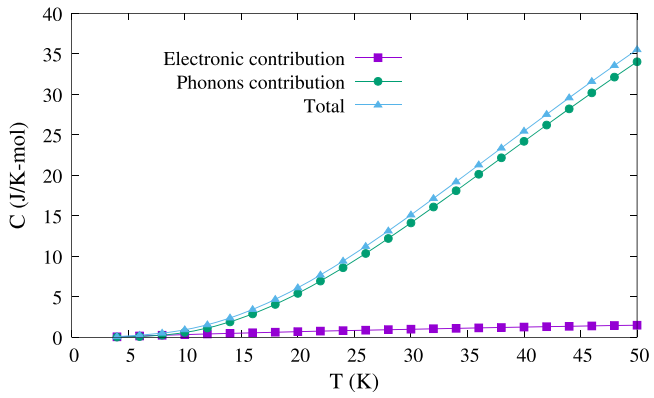

Figure 5. Phonons contribution and electronic contribution to the heat capacity for $CoSb_{2.875}$.

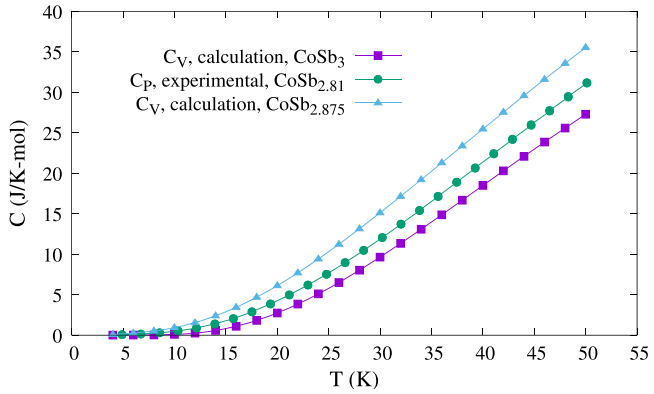

Figure 6. Experimental heat capacity (measured at constant pressure) and heat capacity calculated (at constant volume).

difference between C_P and C_V in the same way justifies the comparison in the same graph of C_P and C_V values, these being almost equivalent at very low temperatures.

4. Conclusions

We discuss the results of *ab initio* calculations obtained by the theory of density functional (DFT) in skutterudites of different compositions. In particular, we report results related to the electronic structure and dynamics of the network. The electronic DOS for the compositions $CoSb_3$, $CoSb_{2.875}$, $CoTe_{0.125}Sb_{2.875}$ and $CoGe_{0.125}Sb_{2.875}$ were reported. Sb vacancies destroy the narrow band gap of $CoSb_3$ making it a conductor. Substitutional Te is an electron donor, while Ge is an electron acceptor. These dopants do not destroy the narrow band gap, but in concentrations similar to those of Sb vacancies, cause similar values of the electric conductivity in order of magnitude. The phonon dispersion curves for the $CoSb_3$ and $CoSb_{2.875}$ compositions were calculated. In both cases the curves are separated into two clearly identifiable groups, although the phonon gap is closed in $CoSb_{2.875}$. Finally, the heat capacity curves as a function of temperature were determined for the two compositions mentioned. These curves were compared with experimental data measured in a sample whose composition is $CoSb_{2.81}$. The predictions of the *ab initio* calculations are reasonably close to the experimental data.

Acknowledgments

The main author thanks the support of CONACYT, especially the financial aid for the postdoctoral project, with proposal number 253354. Powered@NLHPC: this research was partially supported by the supercomputing infrastructure of the NLHPC (ECM-02).

ORCID iDs

Diego Velasco-Soto https://orcid.org/0000-0003-0466-5141

References

[1] Aliabad H R, Ghazanfari M, Ahmad I and Saeed M A 2012 *Comput. Mater. Sci.* **65** 509–19
[2] Lu P X, Ma Q H, Li Y and Hu X 2010 *J. Magn. Magn. Mater.* **322** 3080–3
[3] Sharma S and Pandey S K 2014 *Comput. Mater. Sci.* **85** 340–6
[4] Wojciechowski K T, Toboła J and Leszczyński J 2003 *J. Alloys Compd.* **361** 19–27
[5] Nielsch K, Bachmann J, Kimling J and Böttner H 2011 *Adv. Energy Mater.* **1** 713–31
[6] Sootsman J R, Chung D Y and Kanatzidis M G 2009 *Angew. Chem. Int. Ed.* **48** 8616–39
[7] Rogl G and Rogl P 2017 *Curr. Opin. Green Sustainable Chem.* **4** 50–7
[8] Christensen M, Iversen B B, Bertini L, Gatti C, Toprak M, Muhammed M and Nishibori E 2004 *J. Appl. Phys.* **96** 3148–57
[9] Stoica M and Lo C S 2012 *Phys. Rev. B: Condens. Matter* **86** 115211
[10] Kurmaev E Z, Moewes A, Shein I R, Finkelstein L D, Ivanovskii A L and Anno H 2004 *J. Phys. Condens. Matter* **16** 979
[11] Toprak M S, Stiewe C, Platzek D, Williams S, Bertini L, Müller E, Gatti C, Zhang Y, Rowe M and Muhammed M 2004 *Adv. Funct. Mater.* **14** 1189–96
[12] Liu W S, Zhang B P, Li J F and Zhao L D 2007 *J. Phys. D: Appl. Phys.* **40** 566
[13] Nolas G S, Kaeser M, Littleton R T IV and Tritt T M 2000 *Appl. Phys. Lett.* **77** 1855–7

[14] Harnwunggmoung A, Kurosaki K, Ohishi Y, Muta H and Yamanaka S 2011 *J. Alloys Compd.* **509** 1084–9
[15] Hammerschmidt L, Quennet M, Töpfer K and Paulus B 2015 *Surf. Sci.* **637** 124–31
[16] Giannozzi P *et al* 2009 *J. Phys. Condens. Matter* **21** 395502
[17] Perdew J P, Burke K and Ernzerhof M 1996 *Phys. Rev. Lett.* **77** 3865
[18] Hartwigsen C, Gœdecker S and Hutter J 1998 *Phys. Rev. B: Condens. Matter.* **58** 3641
[19] Goedecker S, Teter M and Hutter J 1996 *Phys. Rev. B: Condens. Matter.* **54** 1703
[20] Standard Solid State Pseudopotentials, (www.materialscloud.org/sssp)
[21] Garrity K F, Bennett J W, Rabe K M and Vanderbilt D 2014 *Comput. Mater. Sci.* **81** 446–52
[22] Dal Corso A 2014 *Comput. Mater. Sci.* **95** 337–50
[23] Madsen G K and Singh D J 2006 *Comput. Phys. Commun.* **175** 67–71
[24] di Meo R, Dal Corso A, Giannozzi P and Cozzini S 2009 Calculation of phonon dispersions on the grid using quantum ESPRESSO *Proc. COST School (Trieste)*
[25] Quantum Design 2004 Physical Property Measurement System: Heat Capacity Option User's Manual. Retrieved from (www.mrl.ucsb.edu/sites/default/files/mrl_docs/instruments/hcapPPMS.pdf)
[26] Realyvazquez-Guevara P R, Rivera-Gomez F J, Faudoa-Arzate A, Botello-Zubiate M E, Sáenz-Hernández R J, Santillán-Rodríguez C R and Matutes-Aquino J A 2017 *Materials* **10** 287
[27] Rahnamaye Aliabad H A, Ghazanfari M, Ahmad I and Saeed M A 2012 *Comput. Mater. Sci.* **65** 509–19
[28] Wee D, Kozinsky B, Marzari N and Fornari M 2010 *Phys. Rev. B: Condens. Matter* **81** 045204
[29] Zhu Y, Shen H, Zuo L and Guan H 2011 *Solid State Commun.* **151** 1388–93
[30] Lu P X, Shen Z G and Hu X 2010 *Physica B: Condens. Matter* **405** 1740–4
[31] Hammerschmidt L, Schlecht S and Paulus B 2013 *Phys. Status Solidi* A **210** 131–9
[32] Koleżyński A and Szczypka W 2017 *J. Alloys Compd.* **691** 299–307
[33] Hanus R, Guo X, Tang Y, Li G, Snyder G J and Zeier W G 2017 *Chem. Mater.* **29** 1156–64
[34] Arushanov E, Fess K, Kaefer W, Kloc C and Bucher E 1997 *Phys. Rev. B: Condens. Matter* **56** 1911
[35] Kraemer A C, Gallas M R, Da Jornada J A H and Perottoni C A 2007 *Phys. Rev. B: Condens. Matter* **75** 024105
[36] Shirotani I, Noro T, Hayashi J, Sekine C, Giri R and Kikegawa T 2004 *J. Phys. Condens. Matter* **16** 7853
[37] Kraemer A C, Perottoni C A and Da Jornada J A H 2005 *Solid State Commun.* **133** 173–6
[38] Koga K, Akai K, Oshiro K and Matsuura M 2005 *Phys. Rev. B: Condens. Matter* **71** 155119
[39] Singh D J and Pickett W E 1994 *Phys. Rev. B: Condens. Matter* **50** 11235
[40] Nolas G S, Slack G A, Caillat T and Meisner G P 1996 *J. Appl. Phys.* **79** 2622–6
[41] Sofo J O and Mahan G D 1998 *Phys. Rev. B: Condens. Matter* **58** 15620
[42] Arushanov E, Respaud M, Rakoto H, Broto J M and Caillat T 2000 *Phys. Rev. B: Condens. Matter* **61** 4672
[43] Nagao J, Ferhat M, Anno H, Matsubara K, Hatta E and Mukasa K 2000 *Appl. Phys. Lett.* **76** 3436–8
[44] Feldman J L and Singh D J 1996 *Phys. Rev. B: Condens. Matter* **53** 6273
[45] Feldman J L, Singh D J, Mazin I I, Mandrus D and Sales B C 2000 *Phys. Rev. B: Condens. Matter* **61** R9209
[46] Ghosez M and Veithen M J 2007 *J. Phys. Condens. Matter* **19** 096002
[47] Volja D, Kozinsky B, Li A, Wee D, Marzari N and Fornari M 2012 *Phys. Rev. B: Condens. Matter* **85** 245211
[48] Kittel C 2005 *Introduction to Solid State Physics* 8th edn (New York, NY: Wiley)